Cessation of the 22–25 June 2006 Coastally Trapped Wind Reversal

DAVID A. RAHN AND THOMAS R. PARISH

Department of Atmospheric Science, University of Wyoming, Laramie, Wyoming

(Manuscript received 1 April 2009, in final form 15 January 2010)

ABSTRACT

Coastally trapped wind reversals (CTWRs) occur periodically in the marine boundary layer off the western coast of the United States and dramatically change the low-level wind regime and coastal weather. Southerly flow becomes established with the passage of a CTWR along with cooler temperatures and a low stratus deck in a narrow band along the coast. CTWRs can propagate northward along the coast for hundreds of kilometers. A strong CTWR commenced in southern California on 22 June 2006 and moved north along the California coastline before stalling at Cape Mendocino on 24 June 2006. A transcritical Froude number differentiates the CTWR layer from the climatologically favored northern wind regime to the north of Cape Mendocino and indicates a barrier to the movement of a density current. A well-defined cloud boundary is present as detected by radar and satellite imagery and sharp gradients exist in the basic-state parameters as measured by instrumented aircraft. As the Pacific high migrates back offshore, the horizontal pressure field near Cape Mendocino becomes increasingly adverse to the continued northward movement of the CTWR layer and typical summertime conditions are reestablished. Observations and modeling results show that the cessation phase of this CTWR was characterized by a surprising lack of topographic blocking due to the mountainous coastal terrain and Cape Mendocino massif. The horizontal pressure field over the ocean to the north of the CTWR was the key impeding force to continued propagation of this event.

1. Introduction

The Pacific high drives low-level northerly flow along the California coast during summer. A coastal jet at the top of the marine boundary layer (MBL) is often embedded in this flow (e.g., Zemba and Friehe 1987; Burk and Thompson 1996; Rogers et al. 1998; Parish 2000; Rahn and Parish 2007). This northerly wind regime is interrupted several times each summer by weak southerly flow adjacent to the coast that is often accompanied by fog or low stratus that moves northward along the coast. These wind reversals have been known as coastally trapped disturbances (e.g., Reason and Steyn 1992), southerly alongshore surges (e.g., Mass and Albright 1987), or coastally trapped wind reversals (CTWRs; e.g., Nuss et al. 2000). Prior to the development of these events, the Pacific high migrates to the northeast thereby increasing the offshore flow component aloft along the coast. As a result of warm air advection and subsidence off the continent, atmospheric temperatures increase dramatically over the coastal waters and the horizontal pressure gradient over the coastal ocean becomes weaker and can reverse (Bond et al. 1996; Nuss et al. 2000; Nuss 2007).

Upon passage of a CTWR, the wind reverses to the south and is accompanied by cooler temperatures and low-level fog or stratus. Clouds generally form within a narrow band adjacent to the coast, which deepens and extends farther offshore to the south. Strong events may propagate hundreds of kilometers along the coastline with typical speeds ranging from 5 to 12 m s^{-1}. Often the head of the CTWR has been observed to surge northward overnight and may stall or even retreat during the day (Mass and Bond 1996). Modeling studies (Reason et al. 2001; Tory et al. 2001; Rahn and Parish 2008) have addressed the issue of diurnal variations in propagation and suggest that topographic variations, cloud-top cooling, and other radiational effects can be responsible for differential movement of the CTWR. Bond et al. (1996) have pointed out that CTWRs along the California coast occur 1–2 times per month during summer although most events are of the weaker, short-lived variety. An alongshore reversal of the dominant wind regime occurs during the warm season all over the world in addition to the western United States. Other areas include the western coast of South America

Corresponding author address: David A. Rahn, Department of Atmospheric Science, University of Wyoming, Laramie, WY 82071. E-mail: darahn@gmail.com

DOI: 10.1175/2010JAMC2242.1

(Garreaud and Rutllant 2003), southern Africa (Gill 1977; Reason and Jury 1990), and the southeastern coast of Australia (Holland and Leslie 1986; Reid and Leslie 1999).

CTWR events occur in an environment where the MBL is capped by a strong inversion and is bordered by coastal terrain with heights extending above the MBL. To a first approximation the fluid system can be represented by a two-layer shallow water system with a lateral boundary. A number of theories have been proposed to explain the propagation phase of CTWRs and are reviewed in detail by Nuss et al. (2000). Cessation of CTWRs has been discussed by several authors within the context of these theories. Dorman (1985) reported a CTWR that was characteristic of a Kelvin wave, and proposed that it stalled south of Cape Mendocino because the mean northerly wind was on the order of the Kelvin wave phase speed. Dorman (1987) reported a CTWR that surged as a gravity current north along the coast of California until reaching southern Oregon. A number of reasons for the cessation were offered including a thinning of the MBL that reduced the speed of the gravity current moving against the northerly flow and large-scale changes in divergence along the coast. Reason and Steyn (1992) provided a theoretical framework for propagating nonlinear Kelvin waves. This included a critical angle for convex coastal topography that indicates whether or not the wave can propagate past the topography. This is used in two cases—one in Australia and one in California—to explain the behavior of the equatorward surge at convex bends in the coastal topography.

With the exception of Burk and Thompson (2004), less work has been directly focused on the cessation of CTWRs (Nuss et al. 2000). Cessation of CTWRs can be associated with topographic features, particularly with Cape Mendocino in northern California, but is not always the case (e.g., Dorman 1987; Mass and Albright 1987; Reason and Dunkley 1993). Nuss (2007) has demonstrated the importance of synoptic-scale forcing on propagation characteristics of CTWRs. In particular, the role of offshore flow at low levels in the atmosphere in shaping the horizontal pressure field in the near-coastal environment is critical for CTWRs to propagate northward. Topography also plays a large role in modifying the nearshore flow (e.g., Reason et al. 2000; Haack et al. 2001).

A strong, long-lived CTWR occurred from 22 to 25 June 2006. It began in southern California and reached Cape Mendocino on 24 June. Four flights were conducted to document this event from 23 to 25 June during the Dynamics and Microphysics in Marine Stratocumulus project. The project took place during May and June of 2006 and was based out of Arcata, California, where the University of Wyoming King Air (UWKA) was stationed. Objectives were first to investigate the links between drizzle, aerosol spectra, and mesoscale (5–50 km) structure and circulations within the marine stratocumulus under prevalent conditions (northerly flow along the West Coast), and second to investigate the structure and forcing of the atmosphere during a CTWR. Observations and an analysis of the forcing during the propagating phase of this event on 23 June are discussed in Parish et al. (2008) and Rahn and Parish (2008). For this case, propagation northward along the coast was best described as a density current. The density contrast was maintained by cloud-top longwave radiative cooling of the CTWR stratus tongue and by the warming of the atmosphere by offshore flow north of the CTWR. The CTWR was at most weakly rotationally trapped, but not enough to force a dynamic response that was responsible for the propagation of the southerly surge. It is considered trapped by the topography in the sense that the density current is simply channeled by the coastal range. This study now explores the cessation of this event at Cape Mendocino occurring over the following 2 days (24–25 June).

Synoptic conditions for this case are shown in Parish et al. (2008) and are typical of the composite synoptic analysis of CTWRs (Mass and Bond 1996; Nuss 2007). Significant features include a high pressure ridge that extends over the Pacific Northwest with resulting offshore flow over central California at the initial stages of the event. As noted by Nuss et al. (2000), the offshore flow is responsible for altering the horizontal pressure field adjacent to the coast. In the CTWR case from June 2006, the bulk of the offshore flow was confined to a region from Cape Mendocino southward to about Monterey Bay. The effect of the offshore flow on the summertime MBL was profound. Within about a day from the commencement of the offshore flow, the typical MBL structure consisting of a well-mixed layer 200–400 m in depth had collapsed. Boundary layer lapse rates show a monotonic increase in potential temperature in excess of 10 K in the lowest couple hundred meters after warm advection of continental air had occurred. Replacement of cool marine air with warmer continental air in a column of air below 700 hPa implies a pressure decrease of up to 4 hPa, similar to estimates in Reason et al. (2001). Thermodynamic changes in the lower atmosphere were linked to modulation of the horizontal pressure field adjacent to the continent for the June 2006 CTWR.

From 1800 UTC 22 June to 1200 UTC 24 June 2006 the southerly surge moved from Monterey Bay to Cape Mendocino. A large transition in the horizontal pressure field was seen at 1200 UTC 24 June near Cape Mendocino. Weak gradients were present to the south and strong gradients existed to the north of the cape (Fig. 1a). During the next 36 h, the CTWR is impeded from further northward propagation and the surface high begins to retreat to the southwest. On the following day the center of the high

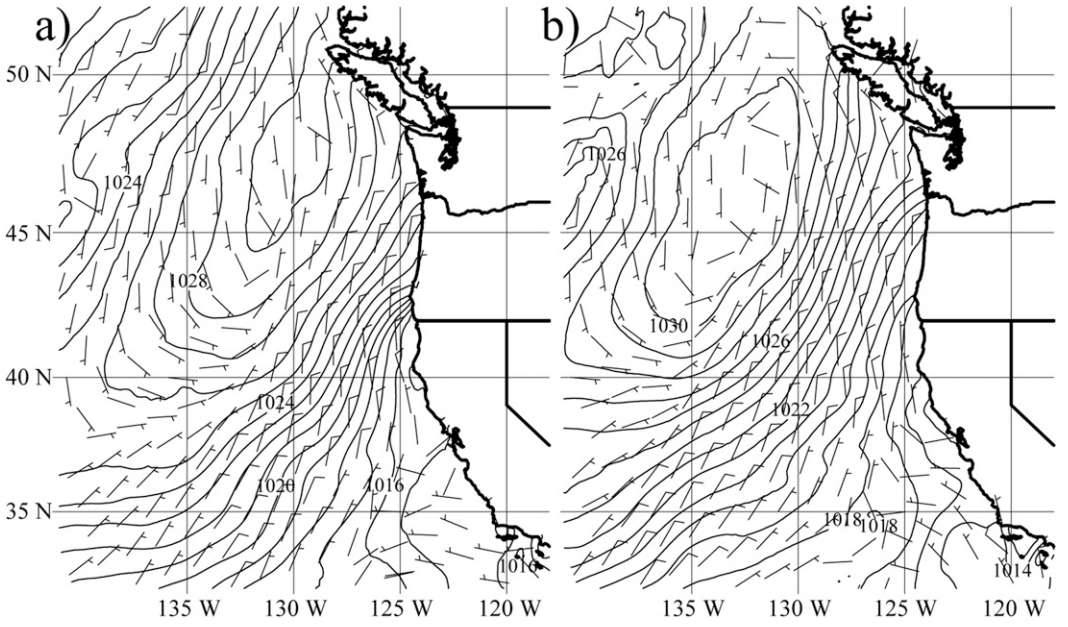

FIG. 1. Sea level pressure (solid; hPa) and 10-m wind (barbs; m s^{-1}) over the ocean from the 12-km NAM analysis grids at (a) 1200 UTC 24 Jun and (b) 1200 UTC 25 Jun 2006.

pressure continues to move to the southwest (Fig. 1b). Associated with this migration of the Pacific high, the pressure gradient near the coast begins to strengthen, the CTWR clouds retreat, and a gradual recovery commences to a more normal summertime setup.

2. UWKA observations from 24 to 25 June 2006

Figure 2 illustrates the sequence of daily 1800 UTC visible satellite images from 22 to 25 June 2006, showing the progression of the stratus finger from south of San Francisco Bay on 23 June to Cape Mendocino on 24 June. Clouds do not progress past Cape Mendocino and the CTWR eventually decays over the next few days. Airborne observations are crucial in diagnosing the CTWR environment and UWKA flights were conducted on both 24 and 25 June 2006. Two flight strategies were used by the UWKA. First, flight legs were conducted in a vertical sawtooth pattern from about 150 to 800 m above the ocean surface along a fixed heading as a means to sample

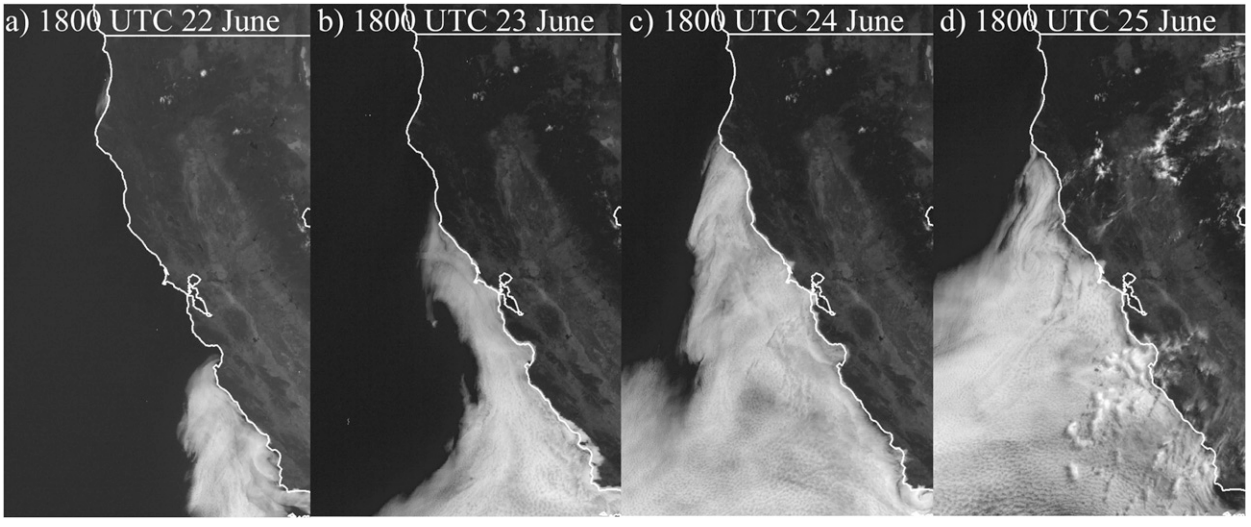

FIG. 2. Visible *Geostationary Observational Environmental Satellite* (*GOES*)-*11* imagery of the CTWR progression along California coast at 1800 UTC (a) 22, (b) 23, (c) 24, and (d) 25 Jun 2006.

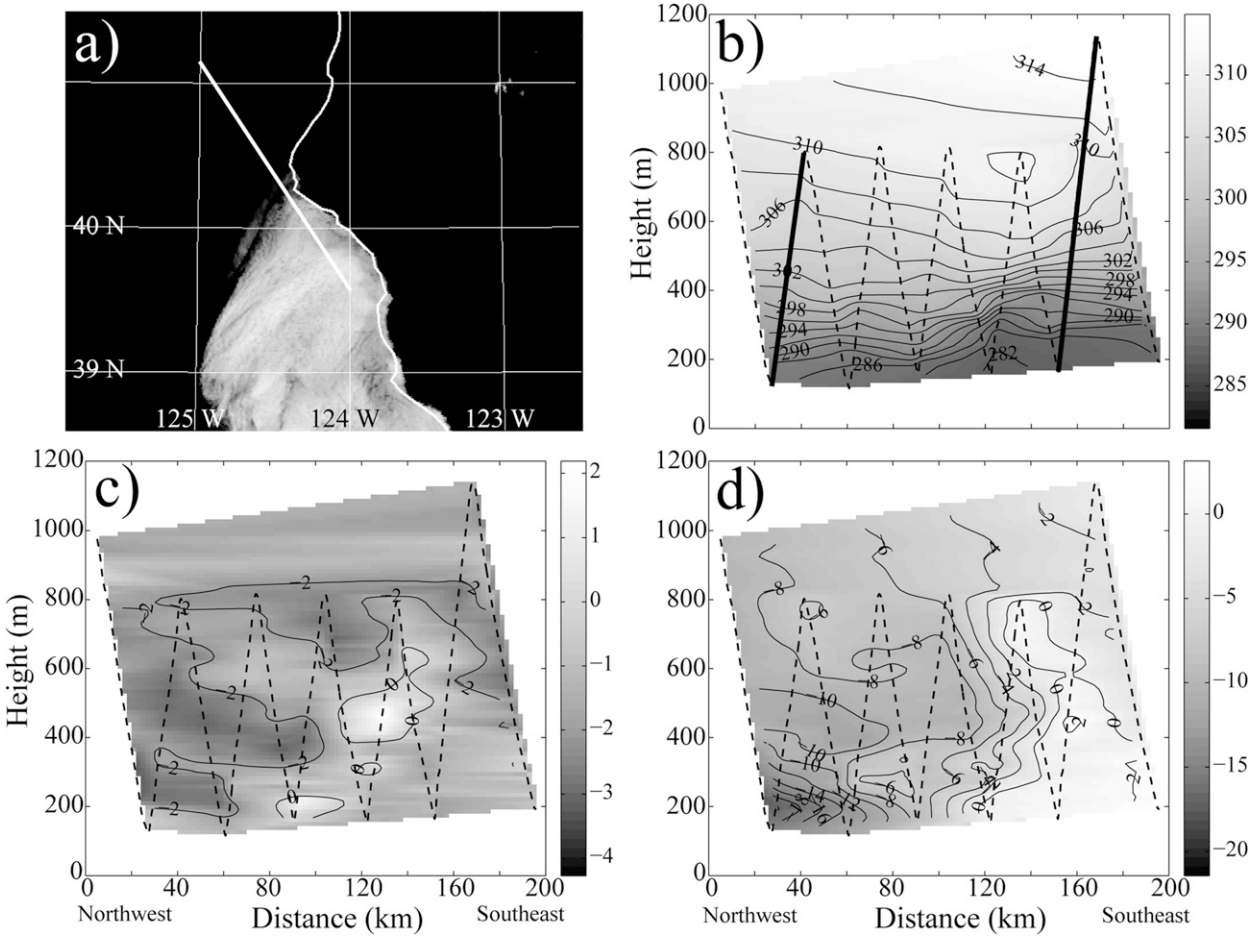

FIG. 3. Sawtooth leg from 1653 to 1735 UTC 24 Jun 2006 showing (a) visible satellite image at 1700 UTC overlaid with the flight track (solid), (b) potential temperature (K; solid, shaded grayscale), (c) zonal wind speed (m s^{-1}; solid and shaded grayscale), and (d) meridional wind speed (m s^{-1}; solid and shaded grayscale). Flight track overlaid as dashed line and locations of soundings in Fig. 4 indicated by thick lines in (b).

the vertical structure of the CTWR environment. A second strategy was to fly along an isobaric surface within the CTWR cloud layer using the autopilot to measure the height of the isobaric surface and hence the corresponding horizontal pressure gradient force (PGF) along the flight path. Details of specific aircraft measurement techniques are provided by Parish et al. (2007). Applications of these types of measurements are demonstrated in Rahn and Parish (2007) and Parish et al. (2008).

The UWKA left the Arcata base at 1630 UTC 24 June and headed over the ocean to the northwest. The first flight leg from 1653 to 1735 UTC was a long vertical sawtooth directed in a roughly southeast direction from a point to the northwest of Cape Mendocino to a point southeast of the cape within the CTWR layer (Fig. 3a). Data from this leg document the transition from the typical summertime northerly wind regime north of Cape Mendocino to the CTWR environment south of the cape. Potential temperatures (Fig. 3b) show the CTWR layer to be cooler than that found to the north and the layer thickness increases to the south. Isentropes show an abrupt rise at the head of the CTWR layer, showing the air within the CTWR layer to be potentially colder than the ambient environment. Depths of the CTWR stratus near the head are about 300 m at a horizontal distance of 120 km on the scale shown in Fig. 3b. The thickness of the CTWR layer has increased by 50 m or so from that found the previous day (cf. Fig. 9 from Parish et al. 2008). Zonal wind components are generally light (<3 m s^{-1}) with offshore flow to the west and above the MBL (Fig. 3c). Meridional components of the wind are shown in Fig. 3d. A northerly low-level jet is present within the MBL to the northwest of Cape Mendocino with observed magnitudes greater than 18 m s^{-1} in the jet core at the far northwest edge of the sawtooth. Immediately to the south of Cape Mendocino, the meridional component of the wind shifts

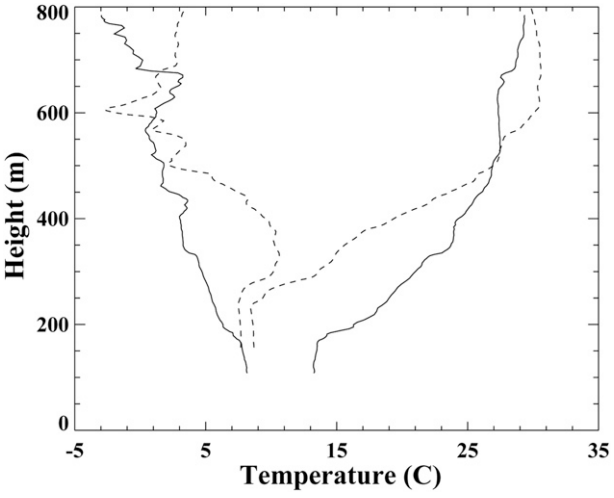

FIG. 4. Vertical profile of temperature (°C) and dewpoint (°C) from the northwest sounding (solid) and the southeast sounding (dashed) from the leg depicted in Fig. 3.

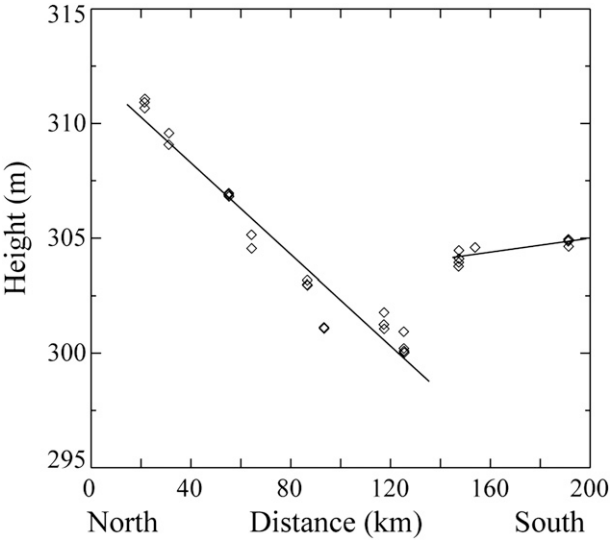

FIG. 5. The height (m) of the 980-hPa interpolated isobaric surface with linear regression lines for the leg depicted in Fig. 3.

to southerly flow associated with the CTWR with magnitudes less than 2 m s^{-1}. The pronounced changes in wind along the flight track imply horizontal convergence is taking place near the head of the CTWR, which is consistent with the upward bulging of the isentropes and deeper boundary layer depth to the south. Cloud-top heights as determined from liquid water content measurement from the UWKA (not shown) indicated an increase from 225 m near the head of the CTWR (about 90 km on the scale in Fig. 3) to 300 m for the last sawtooth descent.

Measurements during the ascents of the aircraft taken from this leg depict the vertical profiles of temperature within and outside of the CTWR layer (Fig. 4; locations of soundings indicated in Fig. 3 by bold lines). The northern sounding (solid) is representative of the typical summertime MBL off the California coast with a relatively warm, unsaturated, and shallow MBL with the inversion beginning just below 200 m. The temperature within the MBL is 13°C. By contrast, the sounding within the CTWR (dashed) shows the atmosphere to be considerably cooler with a temperature near 8°C and near saturation. A strong density contrast at low levels is apparent. Within the CTWR layer, the MBL depth is slightly higher as well. Rahn and Parish (2008) concluded that this density contrast and the relatively flat ambient pressure field to the north of the CTWR layer were responsible for the northward propagation of the CTWR during the previous 2 days.

From this sawtooth leg it is possible to interpret an approximate isobaric surface. This interpolation is done by selecting all points within 0.5 hPa of a specified pressure level (in this case 980 hPa) and then correcting the data to an exact isobaric level using the hypsometric equation. It is recognized that there are relatively few data points compared to isobaric legs to be shown later, but this still gives a fairly representative depiction of the isobaric surface and thus the PGF along the flight path. The interpolated isobaric surface from this first leg is illustrated in Fig. 5. There are clearly two regimes with an abrupt transition in the measurements between 120 and 160 km that mark the head of the CTWR. In the northern half of the leg there is a PGF directed to the southeast with an associated geostrophic wind of approximately 10 m s^{-1}. This component partially supports the strong wind here. Results from the CTWR layer suggest a weak PGF directed to the north in the southern half of the leg with an associated geostrophic wind to the northeast at 2 m s^{-1}. These measurements clearly indicate two different environments. To the north of Cape Mendocino, warm unsaturated conditions are found with relatively strong northerly winds supported by a strong PGF. To the south, the wind is stagnant with a weak PGF and the MBL is about 5°C cooler and saturated. Note the offset in the 980-hPa heights, indicating higher pressure within the CTWR at this time. The presence of a strong, adverse PGF to the northwest of the head of the reversal is significant in the motion of the CTWR.

After completing the initial sawtooth leg, a second sawtooth was initiated at a heading of 275°, cutting across the CTWR layer to the cloud-free environment to the west. Figure 6a illustrates the flight track relative to the stratus extent at that time. Note that the isentropes (Fig. 6b) slope gradually upward toward the east, showing a hint of terrain-induced blocking. This leg reached within about 20 km of the coast and flight notes indicated that

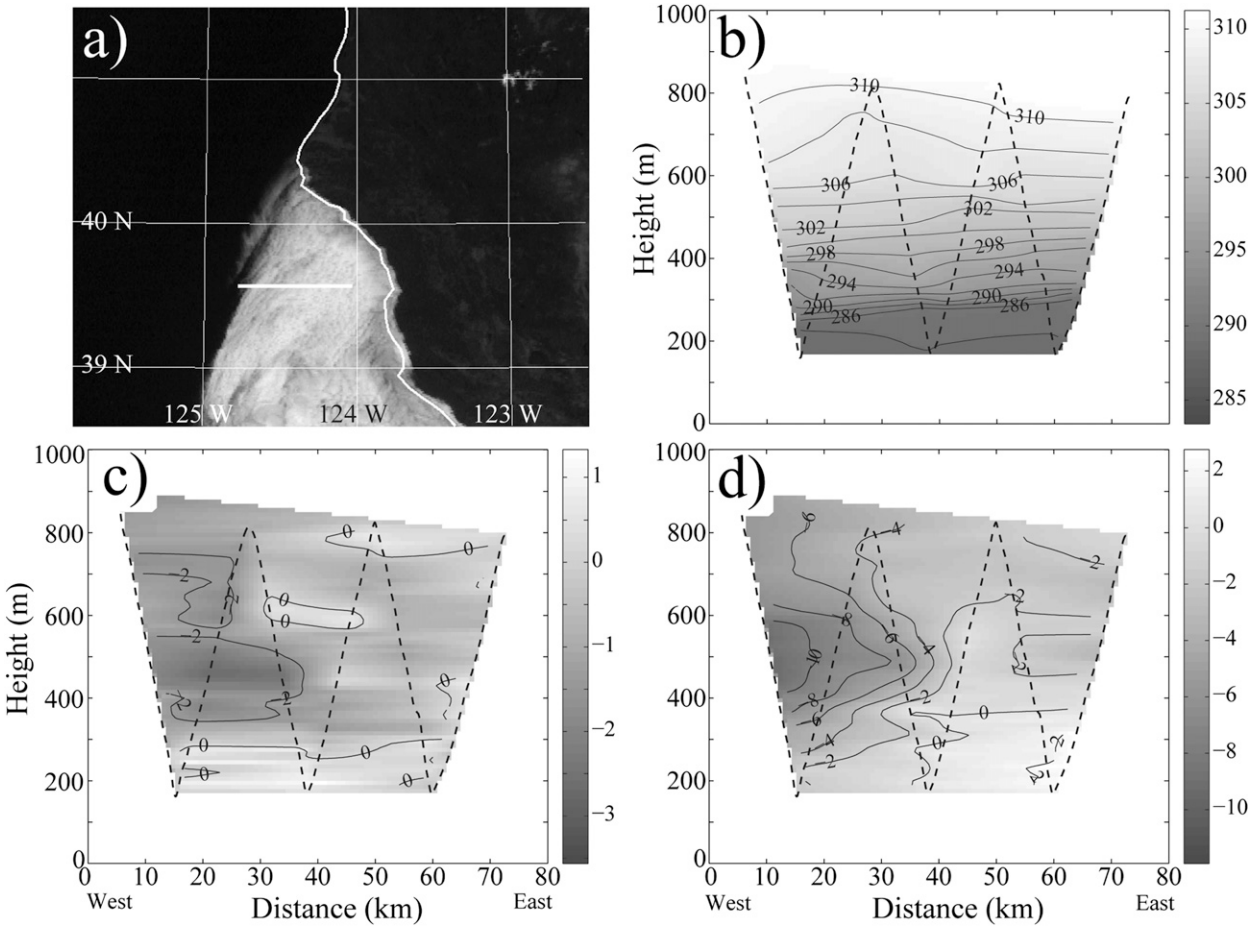

FIG. 6. As in Fig. 3, but for 1745 UTC.

clouds seemed to be less dense near the coast. This can also be seen by close inspection of the satellite imagery. There was little evidence at this time that wind components reflected a barrier influence. Zonal components of the wind (Fig. 6c) were weak throughout the sawtooth. Weak offshore flow at levels below about 500 m was observed to the south of Cape Mendocino during this profiling. Meridional components (Fig. 6d), which are roughly parallel to the coastline, show only weak southerly flow within the CTWR layer shifting to the northerly flow at the far western edge of the leg. Conditions could be best described as tranquil within the CTWR on this leg. Stratus coverage at the lowest portion of the sawtooth profiles made detection of the surface difficult for the most part but at times when the surface could be viewed it seemed to be relatively calm, in contrast to the agitated sea surface state during normal summertime conditions. Cloud-top heights from this leg suggested thicker clouds toward the east, with cloud tops increasing from about 250 m at a distance of 15 km on the scale shown in Fig. 6 to 300 m at the eastern edge.

To continue exploring the possible role of topographic damming, the third leg conducted on 24 June (1755–1814 UTC) was also a vertical sawtooth but with a heading of 45°, roughly normal to the topography just south of Cape Mendocino. It was thought that a path directed at Shelter Cove would have the best chance of observing possible damming features of the CTWR layer at this time. Figure 7a illustrates the flight track for this leg that reached within about 15 km of the coast. In the southwestern half of this leg the MBL depth is near 325 m and decreases slightly toward the northeast (Fig. 7b). Isentropes from this leg display no evidence of topographic damming. As seen in the previous leg, zonal winds are weak with the highest wind speed offshore and above the MBL (Fig. 7c). Figure 7d shows the meridional components within the CTWR layer to be weak as well with southern components indicated only at the lowest section of the last sawtooth profile. To the west stronger north winds associated with the synoptic environment outside the CTWR layer are present with maximum winds about 14 m s^{-1}.

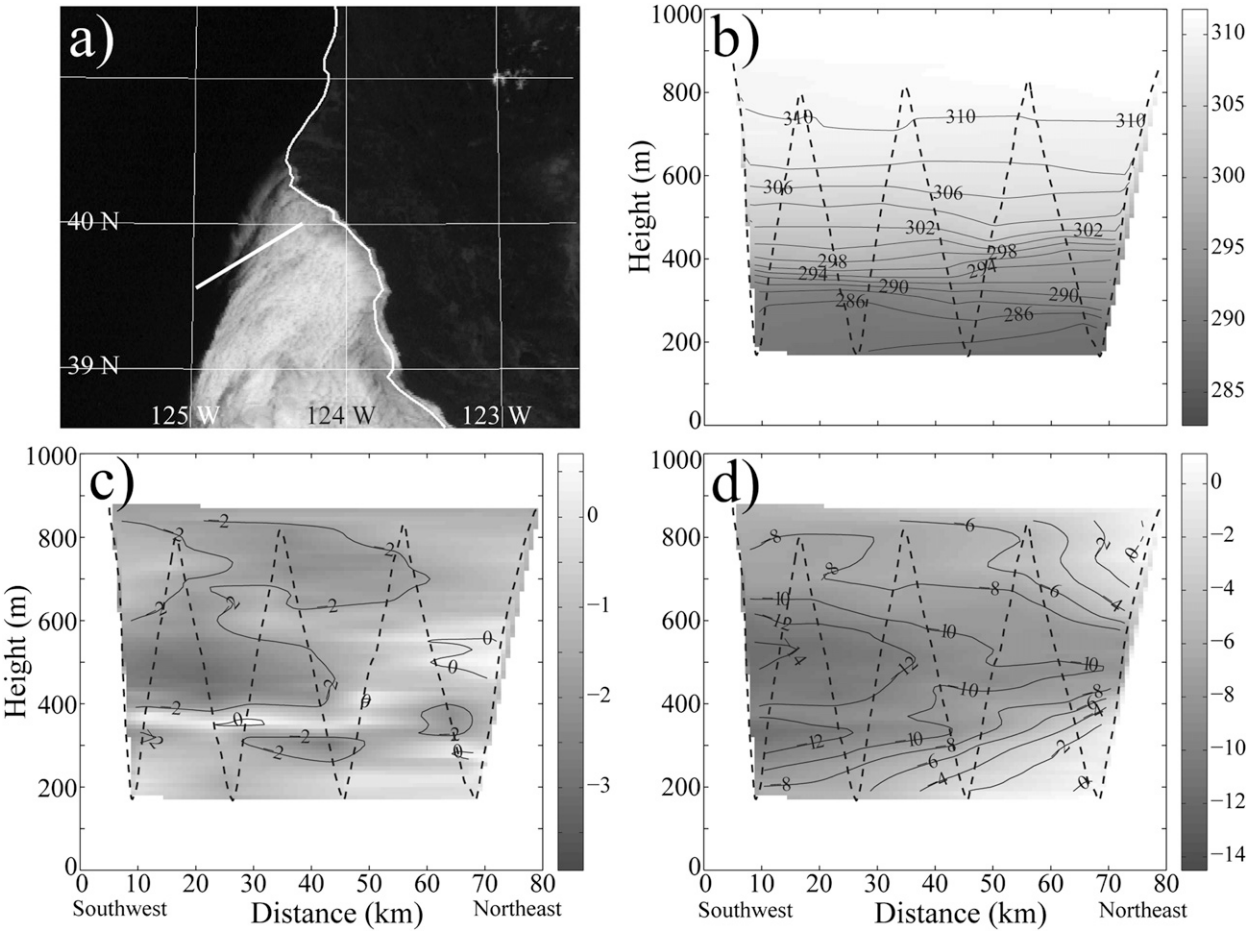

FIG. 7. As in Fig. 3, but for 1755–1814 UTC.

After reaching the northeastern end of the sawtooth near Shelter Cove, the flight strategy was to directly measure the PGF in directions along and perpendicular to the axis of the CTWR stratus. Reciprocal (back and forth along the same path) legs at 996 hPa (corresponding to a level of about 170 m above the ocean) were conducted in directions nearly along the axis of the cloud band in roughly a southwest–northeast pattern. Since cloud-top heights ranged from 250 to 300 m above the ocean, the flight level was well within the stratus layer. Flight rules for the UWKA restricted flight levels to be above 170 m during conditions in which the surface could not be visually detected. As before, the flight leg directed normal to the coast reached within 20 km of the coastline near Shelter Cove (Fig. 8a).

Figure 8b illustrates the heights of the 996-hPa surface during both normal legs. These legs provide the key measurements of the pressure gradient normal to the terrain on this day. Heights along the track were determined using differential correction of GPS position measurements as in Parish et al. (2007). Calculation of the isobaric height was also made with onboard radar altimeters with nearly identical results. The 996-hPa isobaric surface along the southwest portion of the legs outside the CTWR layer has heights that fall to the northeast as would be expected for the normal summertime MBL pressure field. Of interest is the isobaric height trend along the northeast part of the leg within the CTWR. If topographic damming is present, heights should rise toward the northeast. Clouds associated with the CTWR were encountered at about the 45-km mark for the distance scale shown in Fig. 8. Close inspection of the isobaric trace reveals an increase of about 1 m along the flight path within the CTWR layer. For reference, 1 hPa is equivalent to a height change of about 9 m for the density along this leg and thus the horizontal pressure change seen across the stratus at this level is only about a tenth of a hectopascal or so. It can be concluded that topographic damming is not a dynamically significant factor in the motion of the CTWR at this time. Figure 8c depicts the horizontal wind components, showing typical strong northerly flow at the southwest edge of the legs and weak southerly flow associated with the CTWR along the

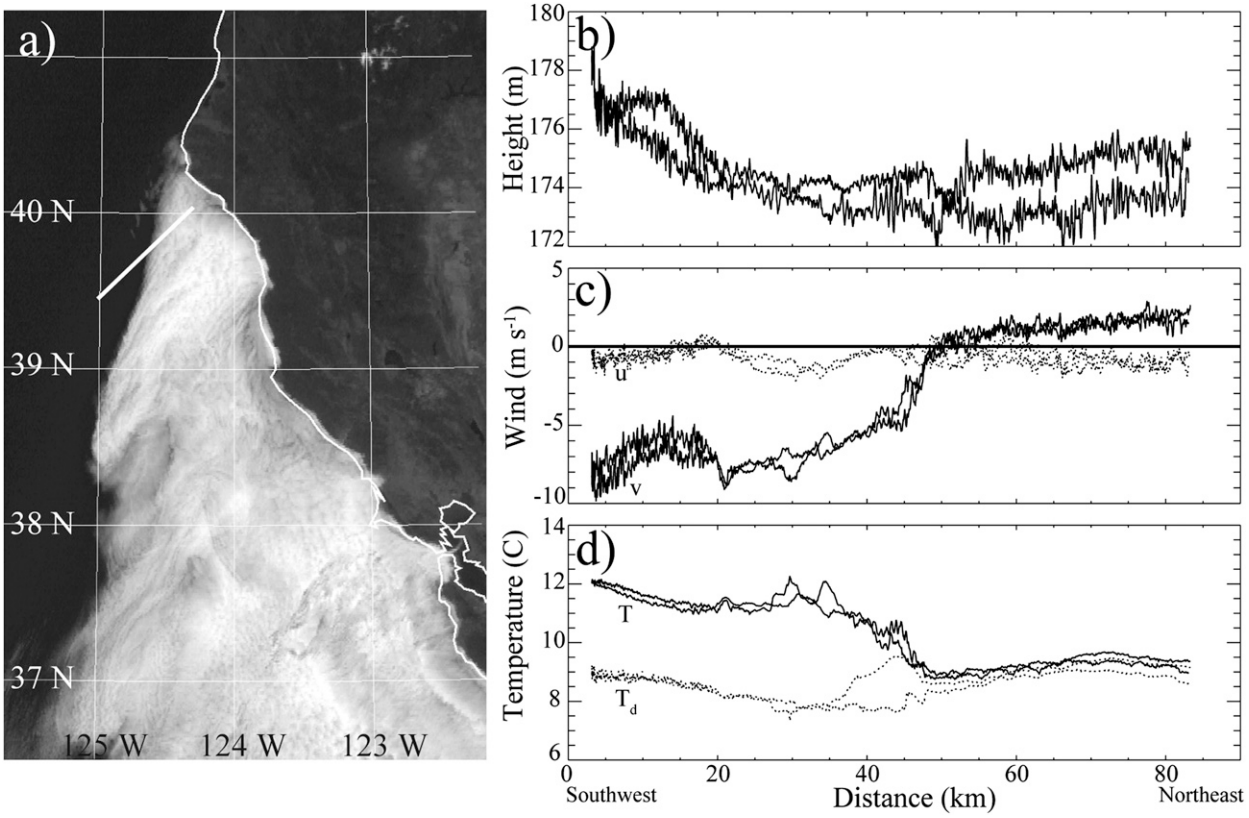

FIG. 8. Reciprocal isobaric legs at 996 hPa from 1859 to 1937 UTC 24 Jun 2006 showing (a) visible satellite image at 1930 UTC 24 Jun 2006 overlaid with the flight track (solid white line), (b) GPS height (m) of isobaric surface, (c) meridional and zonal wind speed (m s^{-1}; solid and dotted, respectively), and (d) temperature and dewpoint temperature (°C; solid and dotted, respectively).

northeastern half of the legs. Temperatures (Fig. 8d) along the isobaric surface show the CTWR to be 2°–3°C colder than the environment away from the coast and hence the cloudy CTWR air can still be viewed as a density current. The lack of northward progress by the stratus tongue cannot be viewed as due to topographic blocking. Rather, it is concluded that the adverse synoptic pressure field found to the north and west of Cape Mendocino restricts movement.

Following the isobaric legs, a return sawtooth leg was conducted from the CTWR layer northwest to a point west of Arcata, similar to the initial sawtooth line. Figure 9a illustrates the flight track. As before, this sawtooth documents the transition from the CTWR layer to the typical summertime MBL structure. Here the head of the stratus is at a distance of about 110 km for the distance scale shown in Fig. 9. Isentropes slope upward to the south at the head of the CTWR layer again indicating the cool air associated with the surge (Fig. 9b). As with all sawtooth legs conducted, isentropic surfaces show the most pronounced changes in a direction along the axis of the cloud layer and especially at the head of the wind reversal. The lack of significant offshore exponential decay of MBL depth and alongshore velocity throughout the period for this CTWR suggests that it is best described as a density current rather than a Kelvin-wave feature. Wind components reveal only weak zonal components to the flow (Fig. 9c) but a marked contrast in the meridional wind (Fig. 9d) from the weak southerly winds within the CTWR layer to the strong northerly low-level jet that is characteristic of the undisturbed summertime MBL.

Satellite imagery indicated that the CTWR stratus retreated slightly during the evening of 24 June. By 1800 UTC 25 June the western edge of the stratus layer south of Cape Mendocino showed a more ragged appearance and the CTWR was dissipating south of Cape Mendocino (Fig. 10a). A final flight was conducted on this day to capture the decay of the wind reversal. This flight consists of one long sawtooth leg flown parallel to the shore, a set of redundant isobaric legs flown in a zonal direction, and a long isobaric leg flown along the shore on the return trip. At this point, the Pacific high is migrating back to the southwest (Fig. 1b). The near-coast pressure gradient is increasing, most importantly south of Cape Mendocino.

The UWKA departed Arcata at about 1650 UTC and conducted an initial vertical sawtooth similar to the day

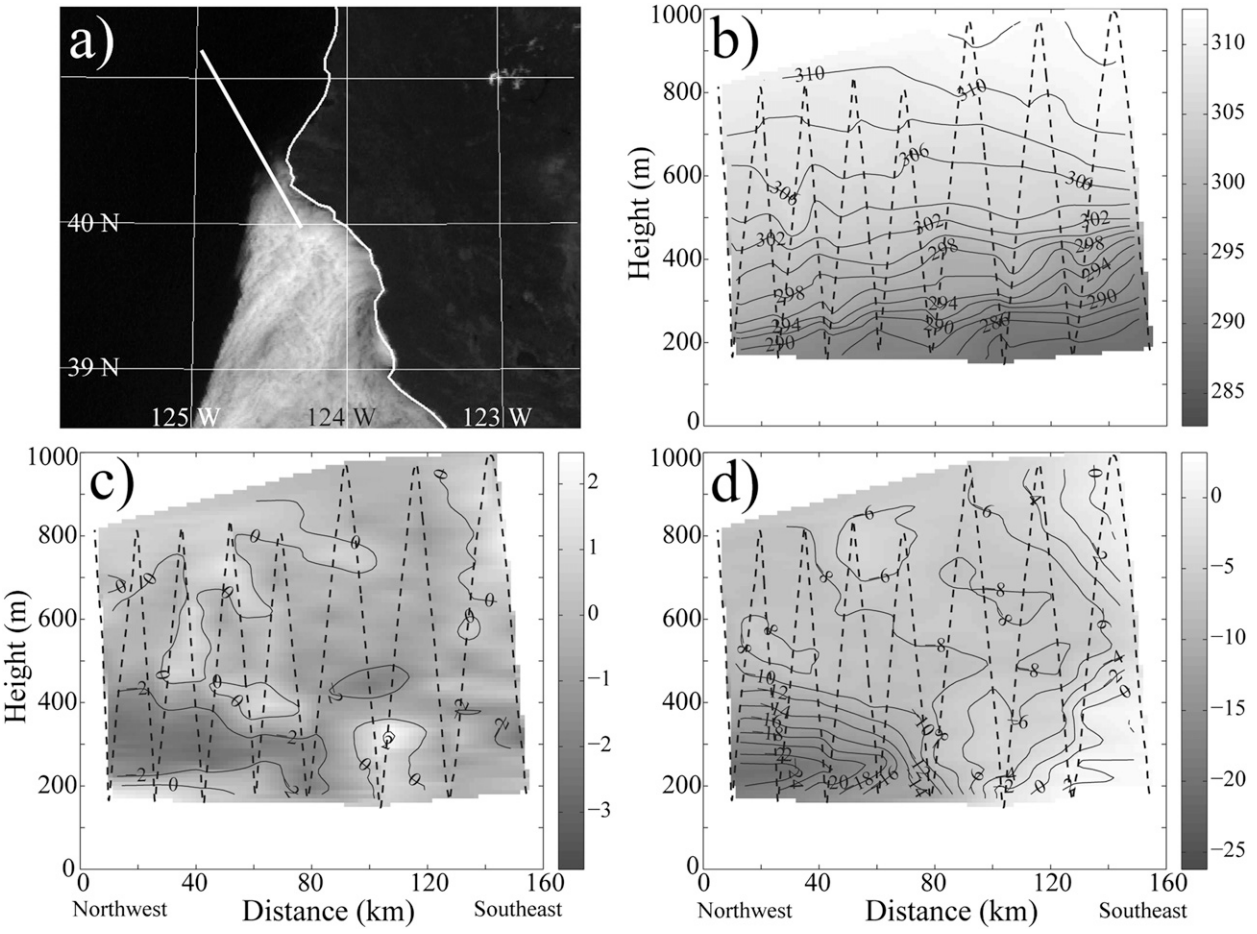

FIG. 9. As in Fig. 3, but for 1937–2015 UTC 25 Jun 2006.

before along a line heading southeast from a point to the west of Arcata to south of Cape Mendocino centered near the northern cloud edge. Figure 10a illustrates the flight track with the CTWR stratus at the time of the sawtooth. The leg covers 200 km and penetrates well into the CTWR. Note the band of cloud at the northern cloud edge. The cross section of the potential temperature again depicts a distinct separation of the MBL to the north and to the south of the cape (Fig. 10b). The MBL is cooler south of the cape with a potential temperature at a height of 200 m near 284 K, while to the north of the cape the potential temperature is near 288 K. The top of the MBL is well defined throughout the leg. There is a local maximum in MBL height just south of the cape at 120 km. Farther south of this peak the MBL decreases and then increases its depth considerably. This local ''bulge'' in the MBL is collocated with the band of cloud in visible satellite imagery. Animation of the visible satellite imagery reveals that this band propagates to the southeast into the CTWR region. The propagation of this particular feature ceases shortly after entering the region south of Cape Mendocino since an MBL that is deeper than the highest amplitude of the wave is encountered.

The zonal wind component is depicted in Fig. 10c. It is generally light (<3 m s^{-1}) over most of the domain, but there is a clear dipole in the zonal flow changing from onshore to offshore near the cloud edge. Onshore flow is associated with the southeast propagation of the cloud band and the offshore component is associated with the flow from the southeast associated with the southerly surge. Between this dipole of zonal flow, the meridional flow (Fig. 10d) shows convergence as the dense CTWR air encounters the northerly wind regime.

Reciprocal isobaric legs were then conducted along an east–west axis at about 160 m above the ocean from 1827 to 1915 UTC. At this time the satellite imagery showed that the CTWR stratuswere displaced from the coast and it was thought that no blocking effects were present. The flight track for the legs is shown in Fig. 11a. The 996-hPa isobaric heights (Fig. 11b) indicate a monotonic decrease to the east with a slightly greater slope along the western half of the leg. Unlike the previous day, clouds associated

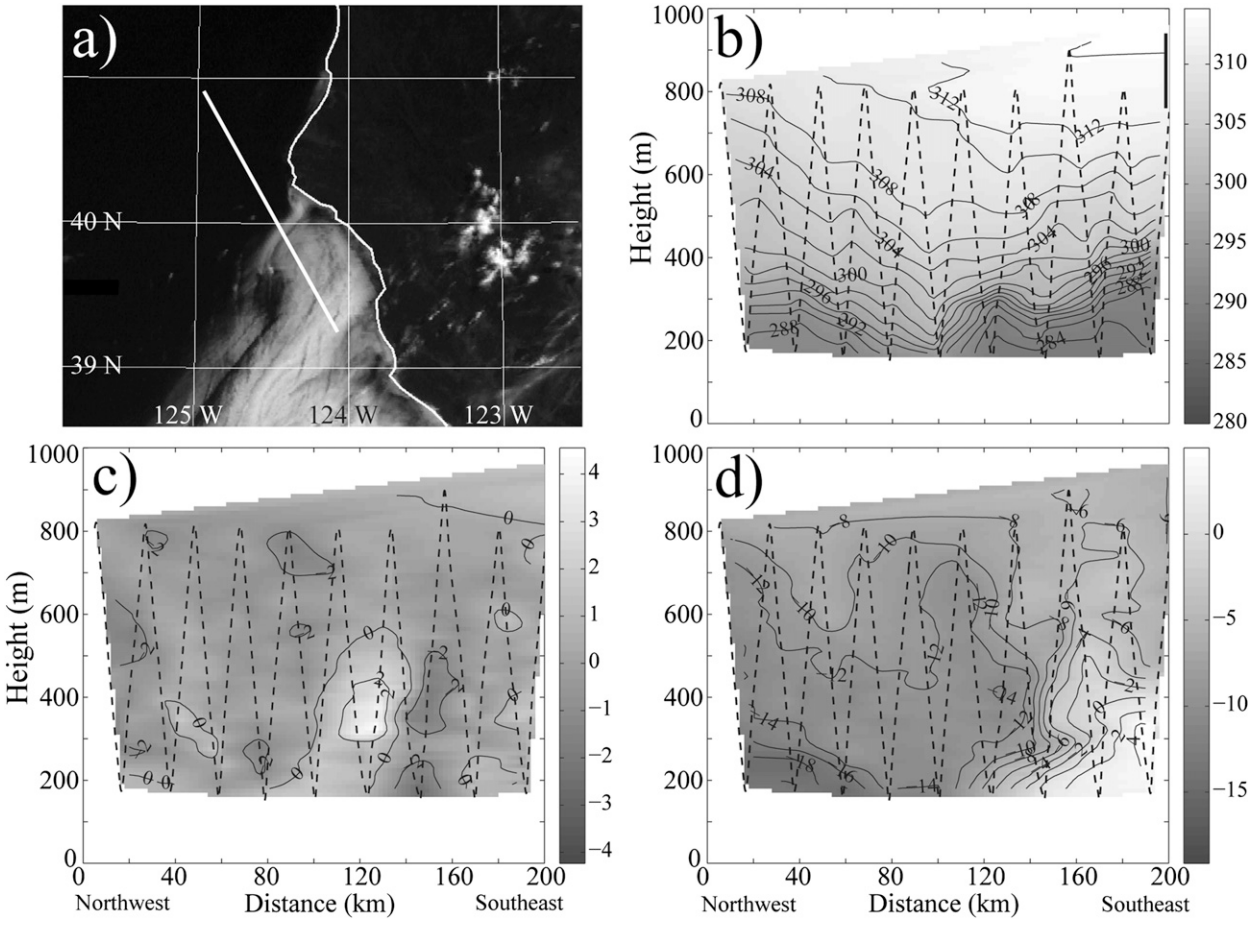

FIG. 10. As in Fig. 3, but for 1739–1822 UTC 25 Jun 2006.

with the CTWR were not uniform and had no well-defined western boundary. At the flight level of about 160 m, CTWR clouds were reached at a distance of about 75 km on the distance scale shown in Fig. 11. Zonal components of wind (Fig. 11c) were quite weak across the entire leg. Meridional wind components illustrate the transition from weak southerlies associated with the CTWR in the eastern part of the leg to the stronger northerly components at the western edge. Temperatures (Fig. 11d) show that the CTWR remains cooler and hence denser than the ambient environment to the west.

The final isobaric leg on 25 June was conducted from 1917 to 1951 UTC along the axis of the CTWR. By this time the CTWR was clearly dissipating. Figure 12a illustrates the flight track for this 140-km leg. Large, coherent variations in the height of the isobaric surface in the northwest portion of the leg just north of the CTWR head are evident (Fig. 12b). At this time the isobaric surface has become significantly perturbed. Southeast of 60 km the height of the isobaric surface has a slight increase toward the south suggesting that a weak northwest-directed PGF exists. A large amplitude wave feature is seen north of the head of the CTWR that flight notes attribute to downslope flow from nearby Cape Mendocino. A second large amplitude wave feature in the isobaric height is seen about the 20-km mark in Fig. 12. The meridional component (Fig. 12c) changes dramatically during this leg from a 5 m s^{-1} southerly component within the CTWR to a 20 m s^{-1} northerly wind over 80 km. Strong temperature perturbations (Fig. 12d) are associated with the local isobaric height perturbations shown in Fig. 12b. Warm anomalies reaching 5°C are evident at 20 and 50 km. Temperatures in the southeastern portion of the leg are steady near 10°C and it can be seen that the CTWR air remains slightly more dense than that found to the northwest.

3. Numerical simulation of the CTWR cessation

Observations from 24 to 25 June 2006 indicate that the CTWR layer remains at a higher density than the environment to the north of the surge layer and retains a northward-directed alongshore PGF. Stalling of the

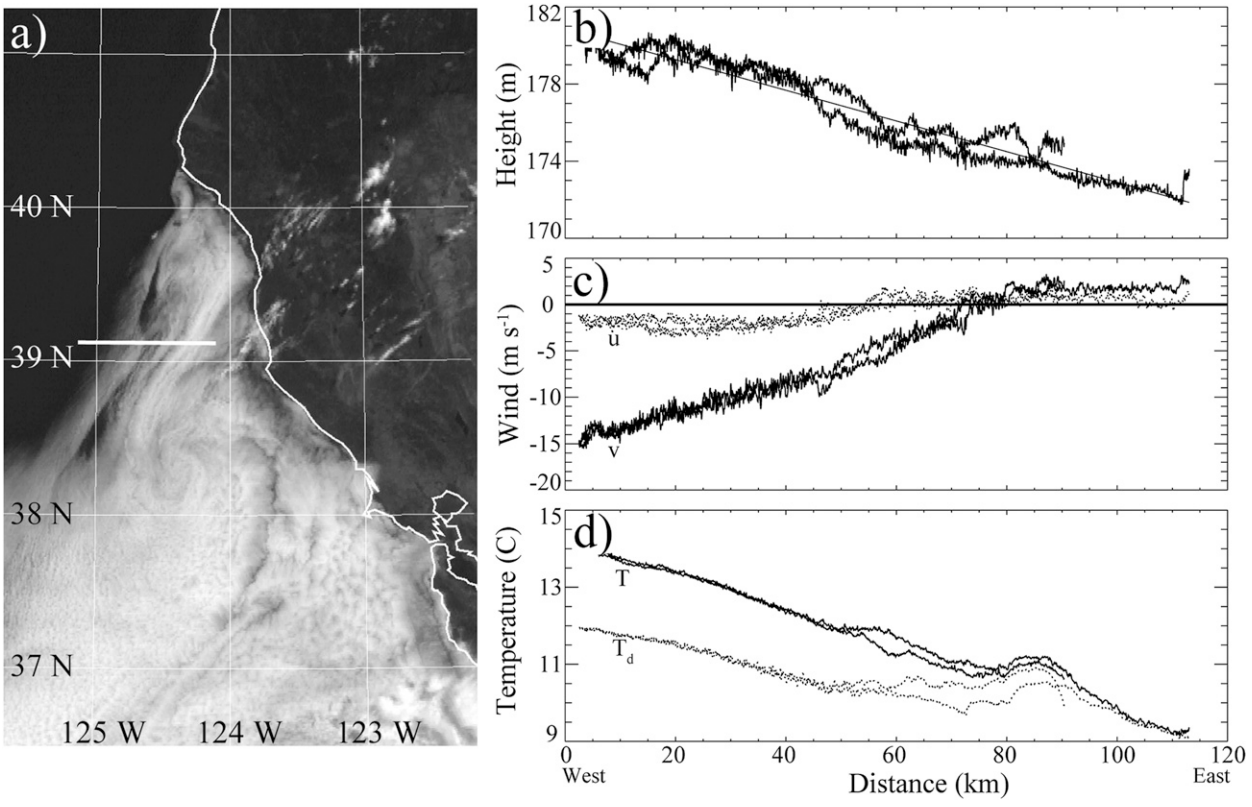

FIG. 11. As in fig. 8, but for 1827–1915 UTC 25 Jun 2006.

CTWR near Cape Mendocino does not appear to be the result of blocking by the steep coastal terrain. This suggests that it can only be that the PGF in the ambient environment is sufficient to prevent further northward propagation of the CTWR. An adverse PGF tends to be present at the end of these events, regardless of the interpretation of the event. Cases where the CTWR stopped at Cape Mendocino (e.g., Dorman 1985; Burk and Thompson 2004) had relatively strong gradients in the surface pressure just north of the cape. In contrast, events that moved beyond Cape Mendocino (e.g., Dorman 1987; Mass and Albright 1987) did not experience adverse pressure gradients until well north of the cape. Observations in the previous section reveal large changes in temperature and wind supported by a strong temperature gradient. To examine the cessation phase, numerical simulations have been conducted using the Advanced Weather Research and Forecasting (WRF model for the 22–25 June 2006 case similar to that described in Rahn and Parish (2008). Details of WRF can be found in Skamarock et al. (2005). The event was modeled using three nested grids with 18-, 6-, and 2-km grid spacing as shown in Fig. 13. Vertical resolution consists of 45 sigma levels with telescoping resolution toward the surface (~10-m resolution near the surface). The parameters used for the run are the following: Thompson microphysics scheme, Community Atmosphere Model (CAM) radiation scheme, Monin–Obukhov (Janjic) surface scheme, Noah land surface model, Mellor–Yamada–Janjic boundary layer scheme, Betts–Miller–Janjic cumulus scheme in the outer domain and none for the inner two domains, second-order turbulence and mixing, and a horizontal Smagorinsky first-order closure eddy coefficient. The model was initialized at 0000 UTC 23 June 2006 using the 12-km North American Mesoscale (NAM) model reanalysis grids and was run for 72 h. The longevity of the southerly surge past 36 h was sensitive to the parameterizations. One of the largest impacts on the simulation was changing both the Rapid Radiative Transfer Model longwave scheme and Dudhia shortwave scheme to the CAM scheme. This greatly increased the longevity of the clouds and the southerly wind near the coast.

Similar to that shown in Rahn and Parish (2008), the WRF simulation is able to capture the northward progression of the stratus finger associated with the CTWR. In agreement with observations, the CTWR stratus stalled at Cape Mendocino on 24 June and began to retreat and dissipate a day later. Here the focus will be on the simulation results near the time of the UWKA observations on 24 and 25 June. Figure 14 illustrates a cross

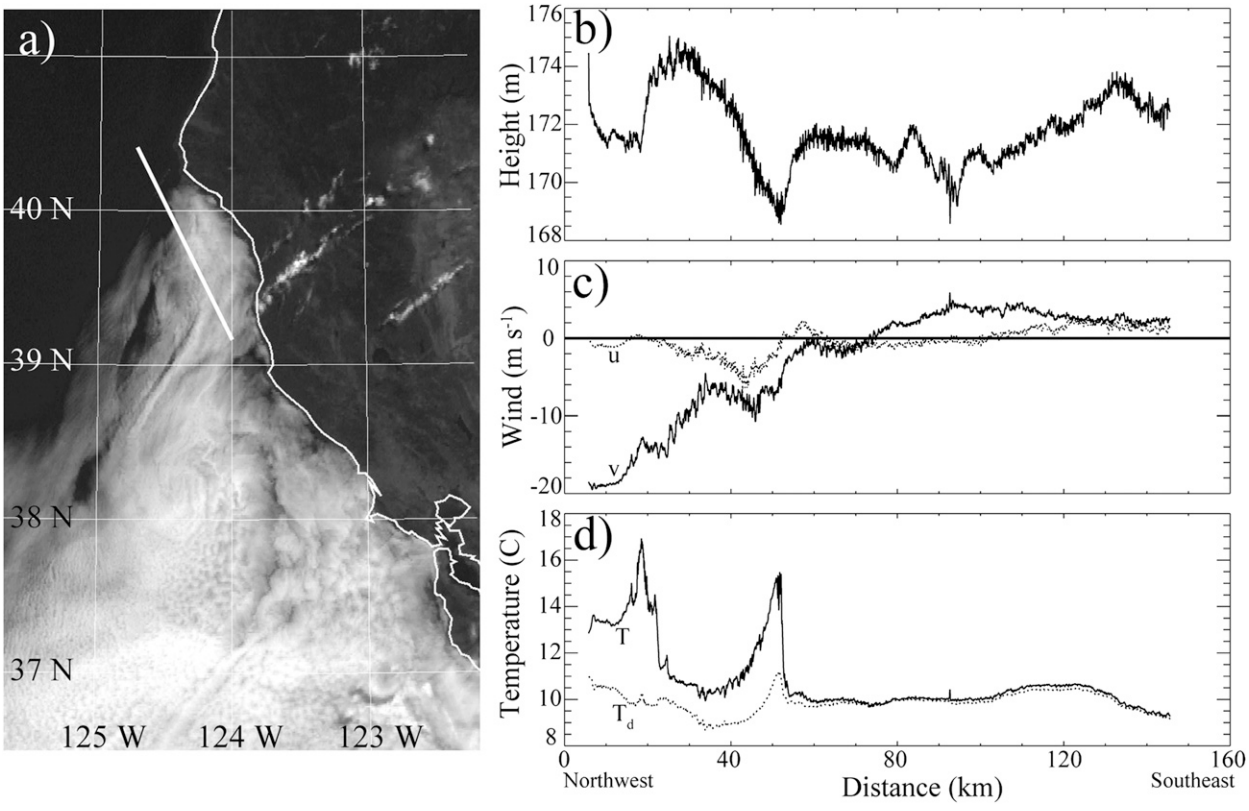

FIG. 12. Isobaric leg at 996 hPa from 1917 to 1952 UTC 25 Jun 2006 showing (a) visible satellite image at 1930 UTC 24 Jun 2006 overlaid with the flight track (solid), (b) GPS height (m) of isobaric surface, (c) temperature and dewpoint temperature (°C; solid and dotted, respectively), and (d) meridional and zonal wind speed (m s^{-1}; solid and dotted, respectively).

section of the WRF simulation at 1700 UTC 24 June 2006, the time and location at which the UWKA was conducting the initial sawtooth leg (Fig. 3). The position of the clouds matches well with observations and is just south of Cape Mendocino. Simulation of the bulging of the isotherms upward near the head of the CTWR roughly matches what is seen in Fig. 3 and the temperatures are consistent with observations. Position and intensity of the low-level jet along the northwestern end of the leg are in agreement with observations. Success of WRF at simulating basic features of the CTWR gives confidence that the physics are being properly represented.

Figure 15 illustrates the height, wind, and temperature fields at the 996-hPa level at 1700 UTC 24 June 2006. This was the level for all isobaric flight legs and thus provides a broad-scale view of the environment sampled during the flight. It can be seen that the temperatures within the CTWR layer and to the west agree with observations. Gradients in temperature right at the western cloud edge such as shown in Fig. 8d are not as well defined in the WRF simulation. While the general horizontal cloud extent matches observations, the thickness of the stratus in WRF is less than observed. Observations indicate that the CTWR stratus extended above 200 m (above 996 hPa) whereas the WRF simulations depict clouds that do not reach past 150 m. Strong temperature gradients are seen adjacent to the western edge of the stratus in the WRF simulation in layers below 996 hPa (not shown). This underscores the importance of the clouds in the simulation of the temperature field associated with the CTWR and the role that cloud-top radiative cooling plays in evolution of the CTWR density (Rahn and Parish 2008). Winds are reasonably well simulated in WRF with winds predominantly from the north ahead of the CTWR and weak southerly flow with the CTWR layer. The horizontal pressure field suggests weak PGF south of Cape Mendocino with stronger gradients to the west outside the CTWR, matching observations from isobaric legs.

Both modeling and observations reveal the vastly different environments north and south of Cape Mendocino. It is clear from WRF simulation results shown in Figs. 14 and 15 as well as observations depicted in Fig. 5 and isobaric legs in Fig. 8 that pronounced density differences exist between the cloudy CTWR air and the ambient environment to the northwest of Cape Mendocino. Despite

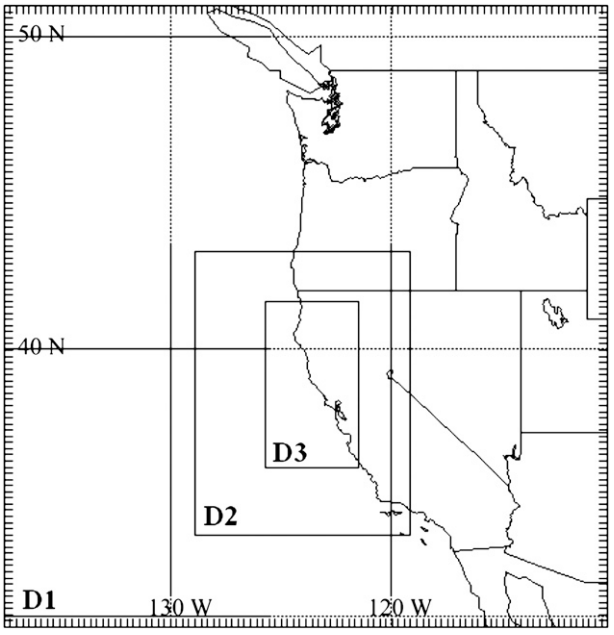

FIG. 13. Model domains used in the WRF simulation. The mother domain (D1), the outer domain (D2), and the inner domain (D3) are bounded by the boxes and correspond to a resolution of 18, 6, and 2 km, respectively.

the density contrast at the head of the CTWR, propagation stalls at Cape Mendocino and it can only be due to the adverse PGF to the north.

An appropriate indicator of fluid regimes is the Froude number (Fr). Specifically, it is the location of the transcritical Froude number (Fr $\sim$ 1) that is of interest. Several studies along the West Coast have used this diagnostic to examine topics such as expansion fans and hydraulic jumps (e.g., Dorman et al. 2000; Haack et al. 2001; Koracin and Dorman 2001; Edwards et al. 2001). This diagnostic has also been applied to CTWRs (Reason and Steyn 1990; Reason 1994; Rogerson 1999; Burk and Thompson 2004). For this application, the Froude number is an important diagnostic in understanding the atmospheric dynamics near Cape Mendocino with special attention given to the phase speed of a gravity wave. From observations it is apparent that the two-layer system near the head of the wind reversal just south of Cape Mendocino is somewhat perturbed, making calculations of the Froude number problematic since defining the scale height is not straightforward (e.g., Burk and Thompson 2004). Notwithstanding this difficulty, calculations of the Froude number do provide quantification that describes the environment.

Burk and Thompson (2004) offered that regardless of how the exact transcritical number is calculated, it is the strong gradients in the Froude number that contain the transcritical line that are the most relevant. For the analysis presented here, the following densimetric form of the Froude number is used:

$$\mathrm{Fr} = \frac{U}{(g'H)^{1/2}}, \quad \text{where} \tag{1}$$

$$g' = g\frac{\Delta\theta}{\theta}, \tag{2}$$

where U is the mean velocity in the MBL, H is the depth of the MBL, g' is the reduced gravity, g is the gravitational force, θ is the potential temperature, and $\Delta\theta$ is the change of potential temperature through the inversion. This form is frequently used and directly relates to the propagation of gravity waves since the denominator represents the speed of the fastest possible propagating internal gravity wave. In a supercritical environment (Fr $>$ 1), gravity waves can only propagate downstream. In a subcritical environment (Fr $<$ 1), gravity waves may propagate freely in any direction since the phase speed, $(g'H)^{1/2}$, is less than the mean free stream velocity (U). Laboratory and numerical studies (Simpson and Britter 1980; Liu and Moncrieff 1996) demonstrate

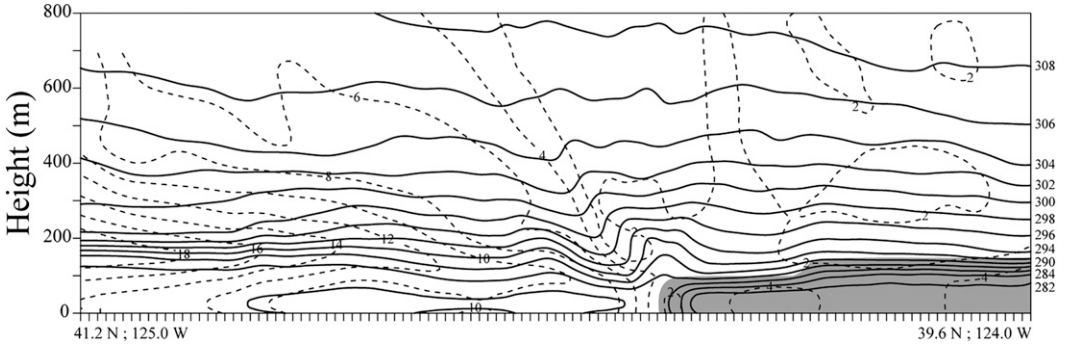

FIG. 14. Cross section from WRF corresponding to flight track in Fig. 3 depicting potential temperature (K; solid contours), wind magnitude (m s^{-1}; dashed contours), and liquid water (gray regions) at 1700 UTC 24 Jun 2006.

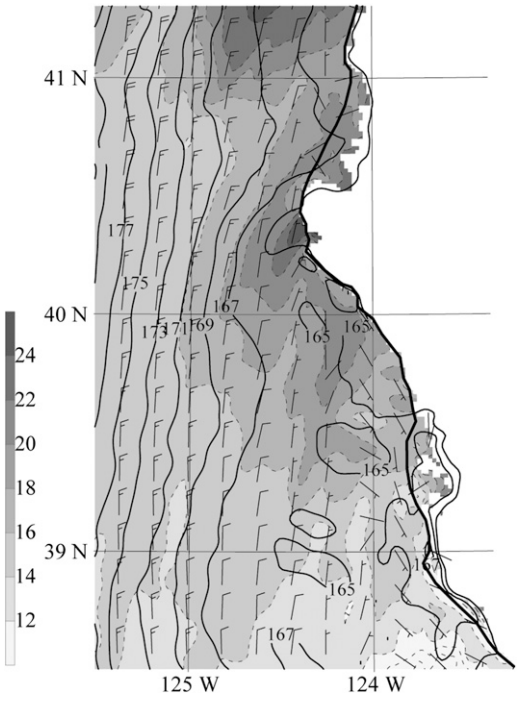

FIG. 15. The 996-hPa height (m; contours), temperature (°C; shaded), and wind (m s^{-1}; barbs) at 1700 UTC 24 Jun 2006.

that propagation of gravity currents within ambient flows is not direct. There is an additional factor (~0.7) that is applied to an opposing flow so that gravity currents may propagate into opposing flows greater than their phase speed. While this may shift the exact line, the large gradients near the transcritical line are still the most relevant features.

For the soundings in Fig. 4, the approximate Froude number is 0.2 for the southern sounding and 1.8 for the northern sounding. While there is a difference in the phase speed between the two regions (10 m s^{-1} in the north and 15 m s^{-1} in the south), the change of the phase speed is small compared to the variation in velocity (18 m s^{-1} in the north and 2 m s^{-1} in the south). Wind speed to the north of Cape Mendocino is supported by a strong PGF that is a consequence of the synoptic signal as modified by the coastal topography. To the south of Cape Mendocino only a weak PGF exists and hence winds are weak. Dominance of the ambient wind speed over the phase speed indicates that the Froude number is really a property of the northerly flow rather than driven by the CTWR. This is yet another indication as to the importance of the synoptic environment for the propagation of the CTWR.

Model results illustrate the Froude number over a larger spatial extent in the region of interest (Fig. 16). A Froude number of unity depicts the transcritical line where a density current cannot propagate upstream. This confinement of the density current movement within the subcritical region is consistent with the movement of the density current on the previous day (Fig. 16a). Note the enhanced gradient of the Froude number that includes the transcritical line. Because the Froude number is less than unity near the coast to the north and south of the cloud

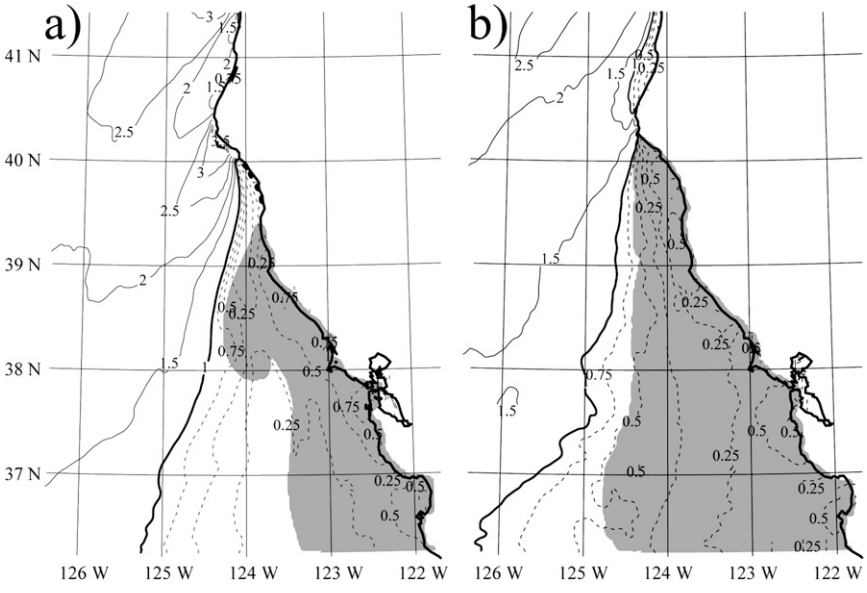

FIG. 16. Cloud (shaded; LWC > 0.02 g kg^{-1}) and Fr [supercritical (solid), subcritical (dashed), and transcritical (thick) contours] at (a) 1900 UTC 23 Jun and (b) 1700 UTC 24 Jun.

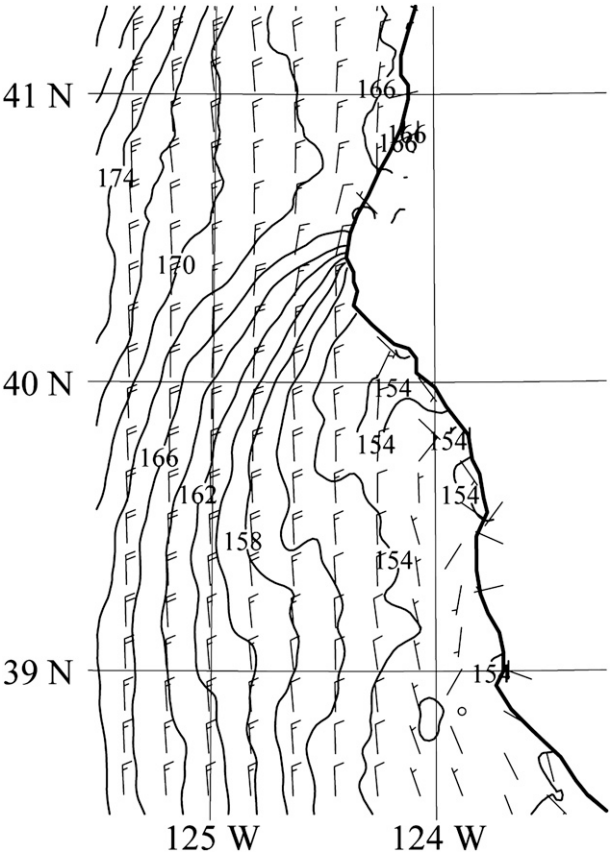

FIG. 17. The 996-hPa height (m; contours) and wind (m s^{-1}; barbs) at 1900 UTC 25 Jun 2006.

layer, the cool and deep layer associated with the CTWR can propagate in either direction. This is seen in the extension of the cloudy regions toward these regions. The gradient in the Froude number in the north is much stronger than the south, highlighting a much stronger demarcation of fluid regimes in the north. Large Froude numbers of around three are seen extending to the southwest of Cape Mendocino at this time, indicating an acceleration of the flow around Cape Mendocino and a thinning of the MBL to the south. This modification of the flow at Cape Mendocino has been attributed to expansion fan dynamics (e.g., Edwards et al. 2001).

Model results also suggest the return of a stronger adverse PGF to the north of Cape Mendocino (Fig. 17) by 25 June. An increased PGF is simulated near and north of Cape Mendocino, which matches what was seen in the aircraft observations. Accompanying this is the stronger wind that heralds the return of the enhanced coastal jet in the lee of Cape Mendocino. The effect of Cape Mendocino on the horizontal pressure field is profound. As the northerly flow at low levels to the north of Cape Mendocino reaches the elevated topography of the cape, significant adjustment of the pressure field occurs. Pressure increases along the north side of Cape Mendocino as the ambient flow is forced against the topography and thereby increases the southward-directed PGF adjacent to Cape Mendocino as seen in Fig. 17. WRF simulations suggest that little blocking of the CTWR air occurs to the south of Cape Mendocino. It can be concluded that the cessation of the CTWR is due to the adjustments in the horizontal pressure field ahead of the CTWR and suggested that propagation is dependent on a favorable ambient PGF in the near-coastal environment. Effects of topographic blocking of the CTWR itself are limited in this case. Weak southerly winds associated with the CTWR remain in a narrow region along the coast. Model results are thus consistent with the notion that propagation of the CTWR on 24–25 June 2006 is limited by the horizontal pressure field in the ambient environment.

4. Summary

After surging north for two days along the coast of California, the CTWR stalls when it reaches Cape Mendocino. For this case the cessation is not linked to topographically induced blocking of the flow but rather to the adverse PGF in the ambient environment ahead of the CTWR. It was surprising that little evidence was found of significant blocking of the CTWR air by the coastal terrain on any of the flight legs conducted during the 23–25 June 2006 period. This demonstrates that for this case no Kelvin wave–type motions exist. The CTWR can be viewed as a density current that is able to propagate northward owing to the flat ambient pressure field in the coastal environment between Monterey Bay and Cape Mendocino. This highlights the importance of the horizontal pressure field on the northward movement of the CTWR.

Rahn and Parish (2008) have shown that a northward surging of the CTWR during nighttime is in large part due to radiative cooling near the top of the stratus layer accompanying the CTWR. Propagation of such a density current, however, can only occur in an environment in which a favorable horizontal pressure gradient force exists. Nuss et al. (2000) have pointed out the importance of offshore flow in the lower levels of the atmosphere as a means to precondition the coastal environment through leeside troughing and/or warm air advection. For this case it appears that warm air advection is the most important factor. Replacement of cool marine air with warm continental air results in a pressure decrease of up to 4 hPa, sufficient to reverse the climatologically preferred north–south pressure gradient. A similar finding along the western coast of South America was also shown by Garreaud et al. (2002), but at a slightly higher magnitude. The synoptic

PGF to the north of Cape Mendocino is typical of the summertime marine layer off the California coast with higher pressure to the northwest—conditions that are adverse to the continued northward movement of the CTWR.

A transcritical Froude number provides a reasonable diagnostic that indicates the CTWR region. Sensitivity of the Froude number to the ambient wind emphasizes the importance of the large-scale flow in impeding the gravity current that is surging against the opposing northerly flow. As the southerly surge associated with the CTWR reaches Cape Mendocino, a strong adverse PGF is encountered as indicated by both UWKA observations and model results. The inability of the CTWR to advance past Cape Mendocino is due to the strong northerly wind and the attendant PGF in the ambient environment. As noted by Nuss et al. (2000), the offshore flow that preconditioned the coastal environment south of Cape Mendocino also implies that the CTWR progression is self-limiting. To the north of the offshore flow near Cape Mendocino, the horizontal pressure field becomes increasingly adverse to continued northward movement of the CTWR.

Acknowledgments. This research was supported in part by the Office of Naval Research through Grant N000140510720 and the National Science Foundation through Grant ATM-0332202. The authors acknowledge Zhien Wang for the additional computer resources to run WRF, pilots Don Cooksey and Kevin Fagerstrom, and scientists Jeff French and Jeff Snider for help with the field measurements.

REFERENCES

Bond, N. A., C. A. Mass, and J. E. Overland, 1996: Coastally trapped wind reversals along the U.S. West Coast during the warm season. Part I: Climatology and temporal evolution. *Mon. Wea. Rev.,* **124,** 430–445.

Burk, S. D., and W. T. Thompson, 1996: The summertime low-level jet and marine boundary layer structure along the California coast. *Mon. Wea. Rev.,* **124,** 668–686.

——, and ——, 2004: Mesoscale eddy formation and shock features associated with a coastally trapped disturbance. *Mon. Wea. Rev.,* **132,** 2204–2223.

Dorman, C. E., 1985: Evidence of Kelvin waves in California's marine layer and related energy generation. *Mon. Wea. Rev.,* **113,** 827–839.

——, 1987: Possible role of gravity currents in northern California's coastal summer wind reversals. *J. Geophys. Res.,* **92,** 1497–1506.

——, T. Holt, D. P. Rogers, and K. Edwards, 2000: Large-scale structure of the June–July 1996 marine boundary layer along California and Oregon. *Mon. Wea. Rev.,* **128,** 1632–1652.

Edwards, K. A., A. M. Rogerson, C. D. Winant, and D. P. Rogers, 2001: Adjustment of the marine atmospheric boundary layer to a coastal cape. *J. Atmos. Sci.,* **58,** 1511–1528.

Garreaud, R. D., and J. A. Rutllant, 2003: Coastal lows along the subtropical west coast of South America: Numerical simulation of a typical case. *Mon. Wea. Rev.,* **131,** 891–908.

——, ——, and H. Fuenzalida, 2002: Coastal lows along the subtropical west coast of South America: Mean structure and evolution. *Mon. Wea. Rev.,* **130,** 75–88.

Gill, A. E., 1977: Coastally trapped waves in the atmosphere. *Quart. J. Roy. Meteor. Soc.,* **103,** 431–440.

Haack, T., S. D. Burk, C. Dorman, and D. Rodgers, 2001: Supercritical flow interaction within the Cape Blanco–Cape Mendocino Orographic Complex. *Mon. Wea. Rev.,* **129,** 688–708.

Holland, G. J., and L. M. Leslie, 1986: Ducted coastal ridging over South East Australia. *Quart. J. Roy. Meteor. Soc.,* **112,** 731–748.

Koracin, D., and C. Dorman, 2001: Marine atmospheric boundary layer divergence and clouds along California in June 1996. *Mon. Wea. Rev.,* **129,** 2040–2055.

Liu, C., and M. W. Moncrieff, 1996: A numerical study of the effects of ambient flow and shear on density currents. *Mon. Wea. Rev.,* **124,** 2282–2303.

Mass, C. F., and M. D. Albright, 1987: Coastal southerlies and alongshore surges of the west coast of North America: Evidence of mesoscale topographically trapped response to synoptic forcing. *Mon. Wea. Rev.,* **115,** 1707–1738.

——, and N. Bond, 1996: Coastally trapped wind reversals along the West Coast during the warm season. Part II: Synoptic evolution. *Mon. Wea. Rev.,* **124,** 446–461.

Nuss, W. A., 2007: Synoptic-scale structure and character of coastally trapped wind reversals. *Mon. Wea. Rev.,* **135,** 60–81.

——, and Coauthors, 2000: Coastally trapped wind reversals: Progress toward understanding. *Bull. Amer. Meteor. Soc.,* **81,** 719–743.

Parish, T. R., 2000: Forcing of the summertime low-level jet along the California coast. *J. Appl. Meteor.,* **39,** 2421–2433.

——, M. D. Burkhart, and A. R. Rodi, 2007: Determination of the horizontal pressure gradient force using global positioning system onboard an instrumented aircraft. *J. Atmos. Oceanic Technol.,* **24,** 521–528.

——, D. A. Rahn, and D. Leon, 2008: Aircraft observations of a coastally trapped wind reversal off the California coast. *Mon. Wea. Rev.,* **136,** 644–662.

Rahn, D. A., and T. R. Parish, 2007: Diagnosis of the forcing and structure of the coastal jet near Cape Mendocino using in situ observations and numerical simulations. *J. Appl. Meteor.,* **46,** 1455–1468.

——, and ——, 2008: A study of the forcing of the 22–25 June 2006 coastally trapped wind reversal based on numerical simulations and aircraft observations. *Mon. Wea. Rev.,* **136,** 4687–4708.

Reason, C. J. C., 1994: Orographically trapped disturbances in the lower atmosphere: Scale analysis and simple models. *Meteor. Atmos. Phys.,* **53,** 131–136.

——, and M. R. Jury, 1990: On the generation and propagation of the Southern African coastal low. *Quart. J. Roy. Meteor. Soc.,* **116,** 1133–1151.

——, and D. Steyn, 1990: Coastally trapped disturbances in the lower atmosphere: Dynamic commonalities and geographic diversity. *Prog. Phys. Geogr.,* **14,** 178–198.

——, and ——, 1992: The dynamics of coastally trapped mesoscale ridges in the lower atmosphere. *J. Atmos. Sci.,* **49,** 1677–1692.

——, and R. Dunkley, 1993: Coastally trapped stratus events in British Columbia. *Atmos.–Ocean,* **31,** 235–258.

——, P. L. Jackson, and H. Fu, 2000: Dynamical influence of large valleys on the propagation of coastally trapped disturbances. *Meteor. Appl.,* **7,** 247–259.

——, K. J. Tory, and P. L. Jackson, 2001: A model investigation of the dynamics of a coastally trapped disturbance. *J. Atmos. Sci.,* **58,** 1892–1906.

Reid, H. J., and L. M. Leslie, 1999: Modeling coastally trapped wind surges over southeastern Australia. Part I: Timing and speed of propagation. *Wea. Forecasting,* **14,** 53–66.

Rogers, D. P., and Coauthors, 1998: Highlights of coastal waves 1996. *Bull. Amer. Meteor. Soc.,* **79,** 1307–1326.

Rogerson, A. M., 1999: Transcritical flows in the coastal marine atmospheric boundary layer. *J. Atmos. Sci.,* **56,** 2761–2779.

Simpson, J. E., and R. E. Britter, 1980: A laboratory model of an atmospheric mesofront. *Quart. J. Roy. Meteor. Soc.,* **106,** 485–500.

Skamarock, W. C., J. B. Klemp, J. Dudhia, D. O. Gill, D. M. Barker, W. Wang, and J. G. Powers, 2005: A description of the advanced research WRF version 2. NCAR Tech. Note NCAR/TN-468+STR, 88 pp.

Tory, K. J., P. L. Jackson, and C. J. C. Reason, 2001: Sensitivity of coastally trapped disturbance dynamics to barrier height and topographic variability in a numerical model. *Mon. Wea. Rev.,* **129,** 2955–2969.

Zemba, J., and C. A. Friehe, 1987: The marine boundary layer jet in the coastal ocean dynamics experiment. *J. Geophys. Res.,* **92,** 1489–1496.